Available online at www.jourcc.com

Journal homepage: www.JOURCC.com

Journal of Composites and Compounds

A review of additive manufacturing of Mg-based alloys and composite implants

Yasamin Zamani [a], Hadi Ghazanfari [b], Gisou Erabi [c], Amirhossein Moghanian [d], Belma Fakić [e], Seyed Mohammad Hosseini [f], Babar Pasha Mahammod [g]*

[a] *Department of Biology, Tehran Medical Sciences Branch, Islamic Azad University (IAU), Tehran, Iran*
[b] *Department of Mining, Metallurgical and Materials Engineering, Université Laval, Québec G1V 0A6, QC, Canada*
[c] *Student Research Committee, School of Medicine, Urmia University of Medical Sciences, Urmia ,Iran*
[d] *Department of Materials Engineering, Imam Khomeini International University, Qazvin 34149-16818, Iran*
[e] *Metallographic laboratory, Institute "Kemal Kapetanović" in Zenica, University of Zenica, B and H*
[f] *School of Mechanical Engineering, College of Engineering, University of Tehran, Tehran, 11155-4563, Iran*
[g] *National Institute of Technology Warangal, Warangal, India*

ABSTRACT

Magnesium based materials are considered promising biodegradable metals for orthopedic bone implant applications as they exhibit similar density and elastic modulus to that of bone, biodegradability, and excellent osteogenic properties. The use of Mg based biomaterials eliminates the limitations of currently used implant materials such as stress shielding and the need for the second surgery. Recently, the development of Mg-based implants has attracted significant attention. Additive manufacturing is one of the effective techniques to develop Mg based implants. Additive manufacturing which could be named 3D printing is a transformative and rapid method of producing industrial parts with in the acceptable dimensional range. Therefore, recent investigations have tried to apply this method for the development of Mg-based implants. This state-of-the-art review focuses on the additive manufacturing of Mg biodegradable materials and their *in-vitro* corrosion and degradation, and mechanical properties. The future directions to develop Mg biodegradable materials are reported through summarization of current achievements.

Peer review under responsibility of JCC Research Group

ARTICLE INFORMATION

Article history:
Received 28 October 2020
Received in revised form 06 December 2020
Accepted 12 February 2021

Keywords:
Additive manufacturing
Magnesium alloys
3D printing
Composite implants

Table of contents

1. Introduction

Since 1988, when the first system (SLA-1) founded on stereolithography (SL) processes was launched, additive manufacturing, rapid prototyping, or 3D printing has been introduced to the market. Since the patent for fused deposition modeling (FDM) was granted in 2009, additive manufacturing technologies started to develop significantly. This technique is already recognized by various names including fused filament fabrication (FFF), 3D printing, or the standard title of material extrusion (ME). The democratization of 3D printing resulted in significant advancements in AM machine software and hardware, as well as the introduction of a diverse variety of construction materials (feedstock used in AM) [1, 2].

The AM technology is applied in many medical applications including customized implants, tissue engineering scaffolds, and anatomical mockups for surgery simulation, planning, and training [3, 4], person-

* *Corresponding author: Yasamin Zamani; E-mail: yasaminzamani181@gmail.com*
DOR: 20.1001.1.26765837.2021.3.6.7.0
https://doi.org/10.52547/jcc.3.1.7

alized surgical guides [5, 6]. As an example, the implants of the metal alloy have been prepared by selective electron beam melting (EBM) or laser melting (SLM), but for anatomical mockups, the processes of SL and PolyJet have been preferred. SLM and EBM according to ASTM F2792-12a, are categorized as technologies of powder bed fusion in which thermal energy fuse specifically powder bed regions [7]. Magnesium alloy due to its comparable mechanical properties, good biocompatibility, and natural degradability, has attracted much attention for application in the bone repair field. Once the Mg implants are placed at the fracture site, the degradation of these implants starts by the electrochemical corrosion mechanism. The released Mg ions contribute to new bone formation and excess magnesium ions will be excreted through the kidneys. In addition, Mg alloy has Young's modulus of approximately 45 GPa as well as density of about 1.79 g/cm^3 which are close to that of human cortical bone (15–30 GPa, 1.75 g/cm^3). However, the fast degradation of Mg leads to excess release of hydrogen gas and structural integrity loss is an important issue [8]. Hence, for a successful bone regeneration, Mg bone-implants should degrade slowly by maintaining good structural integrity and releasing less H_2.

The methodology of additive manufacturing demonstrates much potential in terms of preparing complicated bone implants quickly. Additive processing of Mg-based composites and alloys for the application of bone implants has been studied [9]. Using additive processing, a few researchers prepared Mg-based composites and alloys for bioapplication [10-12]. Due to its capacity for producing biodegradable implants and allowing development possibilities not possible with conventional manufacturing, AM of Mg alloys is gaining prominence in the industry. Magnesium composites have been developed as a potential biomaterial for applications in urology, respiratory medicine, cardiology, and orthopedics. Since the device degrades, the primary benefit of Magnesium is that long-term issues could be reduced or eliminated [13]. Researchers showed that additive produced specimens had stronger mechanical properties and consistency than hot extrude techniques and die cast and base material specimens. In addition, researchers discovered that the mechanical properties of 3D printed Magnesium specimens were superior to those of base materials. [14].

This article reviews the application of additive manufacturing in the preparation of Mg-based materials for bone implants. Besides, the properties of additively manufactured Mg-based materials such as composite's corrosion behavior, in-vito biodegradability, biocompatibility, and mechanical properties are reported and finally, the recent advancements in additive manufacturing are discussed as well.

2. Application of biodegradable Mg alloys in orthopedic implants

In biomedical research, biodegradable metals including Mg, Zn, and Fe have attracted significant attention. Many researchers have been carried to develop biodegradable materials using these metal alloys. Mg and its alloys are the lightest structural alloys, with appealing properties like good damping capacity, high strength to weight ratio, good castability and machinability, and a wide range of uses in industries including aerospace defense, automotive, and electronics [15]. In the physiological medium, however, pure Mg has very low corrosion resistance. Copper, zirconium, manganese, zinc, aluminum, and silicon are used to enhance the corrosion resistance and mechanical characteristics of pure Mg alloys. [16, 17].

Cast magnesium composites are the most popular magnesium alloys used currently in the automobile industry's powertrain and interior parts. Wrought magnesium alloys, on the other hand, are less commonly utilized due to their high cost and low formability [18]. In cast magnesium alloys, rare earth elements such as Gd, Ce, Y, and Nd are used as main alloying components These materials have a high magnesium solubility and are efficient in creep resistance and precipitation hardening [19]. The prevailing cast Mg alloys are Elektron 21, WE43, WE54, QH21, QE22, HZ32, HK31, ZC63, ZE41, ZK61, ZK51, AM50, AZ91, AZ81, and AZ63 while typical wrought Mg alloys are ZC71, ZE41, HM21, HK31, M1A, ZK60, Elektron 675, AZ80, AZ61, and AZ31. Z (Zinc), W (Yttrium), T (Tin), S (Silicon), R (Chromium), O (Silver), N (Nickel), M (Manganese), L (Lithium), K (Zirconium), H (Thorium), F (Iron), E (Rare earth metals), D (Cadmium), C (Copper), B (Bismuth), and A (Aluminum) are the prefix letters for two main alloying metals in Mg composites formed based on ASTM B275. [20].

In biomedicine applications, the generally practiced technique for controlling the Mg degradation rate is alloying. Magnesium can be effectively modified by alloying with an additional suitable amount of other elements to boost its mechanical properties and resistance [21]. Mg alloys are classified into two main categories: austenite and hypereutectate. Magnesium alloys are classified into two major categories. The first category contains between 2 and 10% wt% Al with a small amount of Zn and Mn, showing increased tolerance and mechanics. The second group is the combination of scarce earth elements and another metal including Ag, Zn, Y, and a lesser amount of Zr, leading to improved degradation resistance, finer grain structure, and mechanical performance [20]. Most researches showed that alloying is an appropriate method to control the Mg degradation rate but it does not influence its fundamental qualities. As an example, AZ31B, formed using mixing Al, Zn, and Mg and led to the improvement in the degradation resistance inside the rabbits' femora [22].

Hampp et al. [23] investigated the LANd442 alloy, which is composed of 2 wt percent Nd, 4 wt percent Al, 4 wt percent Li, and 90 wt% Mg. In the examined rabbit model, the results revealed an increase in corrosion resistance with the formation of new bone tissue. A small quantity of subcutaneous gas was also found in the area of the implant. Wu et al. [24] investigated the influences of alloying various amounts of Al and Li on the Mg–Li–Al–Zn quaternary alloy system. Their results revealed that alloying with Li considerably enhanced the ductility while Al improved the Li–Al–Zn alloys strength. The experiment of indirect *in vitro* cytotoxicity exhibited lower cytotoxicity for the alloys showing higher corrosion resistance. *In vivo* corrosion rates in the mouse subcutaneous model demonstrated different corrosion rates than the *in vitro* tests.

According to Li et al. [25], adding <2wt% Sr to Mg–Sr and Mg–Zr–Sr alloys significantly improved corrosion resistance. The addition of Sr improves the corrosion resistance of Mg–5Al alloys. Bone development may be aided by incorporating calcium into magnesium alloys, and the corrosive and mechanical characteristics of Mg–Ca alloys can be regulated by varying the amount of calcium. The dual Mg–Ca alloy of 1-20wt% Ca was tested by Li et al. [26], and the alloy of Mg–1Ca demonstrated no cell toxicity. The corrosion resistance of the Mg–1Ca alloy was increased due to the creation of an apatite layer on the surface. Comparably, Rad et al. [27] discovered that increasing the Ca content of Mg by 0.5 percent improved corrosion. The biodegradable magnesium alloys with different compositions were studied and revealed no favorable results. The appropriate choice of the content and the type of the alloying element can remarkably enhance the Mg without compromising its mechanical function and biocompatibility.

Magnesium and its composites have received a great deal of recognition for temporary implant applications such as screws, orthopedic bone plates, and coronary stents. Ghanbari et al. [28] investigated the wear behavior of biodegradable Mg–5Zn–1Y–(0–1)Ca alloys in simulated body fluid. Because of the improved corrosion resistance caused by the formation of intermetallic Ca2Mg6Zn3 particles, the friction coefficient and wear rate of the Mg–5Zn–1Y–1Ca alloy show more instability than the other alloys. In general, Ca-free alloy gives the best wear resis-

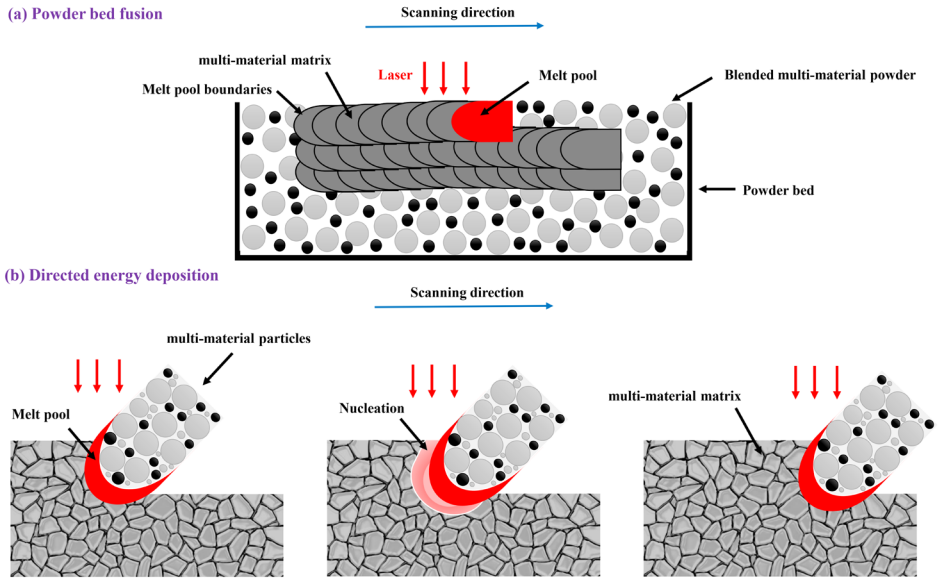

Fig. 1. DED and PBF additive manufacturing.

tance, particularly at the higher load of wear. Wang et al. [29] applied magnesium alloy (Mg–Zn–Y–Nd) stent in esophageal cancer therapy. In comparison to 317 L stainless steel, the Mg alloy inhibited the growth of esophageal cancer cells and had a milder hardness and good biodegradability. In addition, Liu et al. [30] studied the fatigue behavior of an extruded Mg–Zn–Y–Nd alloy for vascular stents in simulated body fluid (SBF) and air. Their findings indicated that the as-extruded alloy of Mg–Zn–Y–Nd in the air has a fatigue limit of 65 MPa after 10^7 cycles, and it has a linear association between stress amplitudes and fatigue life as well, and with no limit in SBF. Zhao et al. [31] investigated the use of pure magnesium screws to fix a vascularized bone graft in patients with femoral head osteonecrosis (ONFH). The findings indicated that using a magnesium screw to support a bone flap is both efficient and biocompatible. The rate of biodegradation is tolerable in comparison to the rate of tissue healing, and the discharged magnesium ions promote new bone formation. Airway stentings can be made from a variety of materials, including hybrid tubes and silicone. These stents, however, do not provide adequate long-term efficacy. Metallic stents, as well as mucociliary clearance, resulted in unfavorable tissue growth and drastic granulation. The large percentage of these side effects necessitates the use of secondary surgical methods to remove the stents. Because of a clear shortage of currently existing stents, there is a significant therapeutic need for biodegradable airway stents that would maintain airway patency and then be completely degrade overtime after achieving the intended goals [32].

The effectiveness of biodegradable Mg composites for the application of tracheal stents was investigated by Wu et al. [33]. This research reveals that magnesium alloys (Mg-Al-Zn-Ca-Mn) have excellent cytocompatibility and that (Mg-Al-Zn-Ca-Mn) is a useful choice for tracheal stent applications. Magnesium and its composites are sorts of biomaterials that, with proper manufacturing and design, will play a significant role in innovating biomedical applications. Wei et al. [34] implanted $COOH^+$ ion to decrease the ZK60 Mg alloy degradation and enhance its application in the physiological environment. *In vitro* cytotoxicity tests and corrosion, experiments show that the treatment of ion implantation can improve the alloy biocompatibility and reduce the corrosion rate. Dai et al. [24] performed Ti, Ni, and Ti/Ni plasma immersion ion implantation on the AM60 Mg composite. In a 3.5 percent solution of NaCl, the corrosion resistance of the Ni- and Ti/Ni-implanted AM60 samples was significantly reduced.

3. Additive manufacturing of Mg-based alloys and composite implants

AM, 3D printing, and solid free-form fabrication are interchangeable terms, and they've been used to create complex 3D porous architectures with precise pore topology control [35]. AM may create a variety of scaffolds with complex geometries that can improve cell diffusion and extracellular matrix (ECM). It uses a layer-by-layer preparation method based on computer-aided design (CAD) models [36]. Depending on the heat source (arc, electron beam, or laser), wire or powder, and feedstock materials used, different kinds of additive manufacturing procedures exist. As shown in Fig. 1, ASTM Standard F2792 categorizes additive manufacturing processes into two categories: powder bed fusion (PBF) and directed energy deposition (DED) [20]. PBF is one of the near net shape strategies of preparation [37] and the most preferred method of additive manufacturing for the fabrication of metallic scaffolds. It uses thermal energy to preferentially fuse and melt metal powders together in layers in a powder bed to produce solid patterns using multiple techniques such as EBM and SLM [38]. The first study on the efficacy of laser powder bed fusion (L-PBF) of magnesium powder was published by Ng et al. [39]. In an insulating gas atmosphere at atmospheric pressure, a mini L-PBF system with a Nd: YAG laser was used to melt single tracks of pure magnesium powders. Great regions of sintered powder were noticed around the tracks, expelling from the molten pool due to extreme evaporation. Oxidation occurs within the track and afterward, the same team investigated the influence of manufacturing variables on the microstructure and structure efficiency of pure magnesium powders using multi-layer melting [40].

3.1. Selective laser melting (SLM)

SLM applies a fiber laser system for energy supply. The entire process occurs in a chamber consisting of inert gas to diminish the surrounding oxygen and decrease absorption of hydrogen, thereby maintaining high purity. Fig. 2 represents a schematic of the SLM system. SLM's fiber laser has a power output of up to 1 kW, depending on the package used in the device [7]. The galvanometer keeps track of the beam's focus, whilst the F-theta changes the beam's displacement on

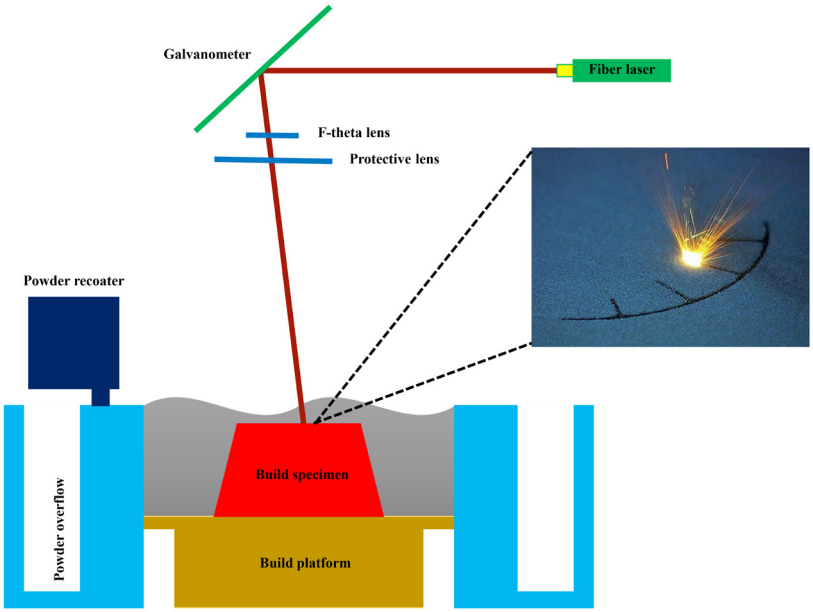

Fig. 2. Schematic illustration of an SLM system.

the build table. The powder reactor carries and spreads a 20-100 mm thick powder film on top of the table. The build table can be preheated up to 200 degrees Celsius. The laser selectively melts the powder layer according to the geometry defined in the CAD file. Each layer of a component is built in two steps using SLM. The part's surface boundaries are first formed, which is referred to as contouring, and then the powder within the contour is melted to create a full single layer. This process continues until the entire three-dimensional template is finished [41]. Applications of SLM are manufacturing orthopedic implants such as zygomatic bone replacements [42] and finger [43].

In fabricating metallic biomaterials, SLM is the most popular technology for powder bed fusion. In SLM, rapid heating and cooling processes exist which normally surpasses 105 K/s [44]. Hence, because of such cooling haste, solidification happens quickly and the grain growth is prevented [45]. Moreover, it decreases the heterogeneity of the composition due to a cohesive microstructure across the substrate. Concerning stage dynamics and grain size, the compact and homogeneous microstructure prefers improved stability, densification, and mechanical properties. Typically, except when a multi-material compound is provided in advance, using one single powder bed dispenser for a single metal powder is challenging in the process of *in-situ* delivery of several substances [46, 47].

Multi-material design using mixed metal or metal-ceramic powder mixtures in the powder bed, SLM has been applied to multi-material production of Mg-based [48-50] and Ti-based [51, 52] biomaterials. The correlation between Mg-Zn structure, deficiencies, and mechanical properties was examined during in situ adsorption of Magnesium combined with Zinc during SLM [51]. The magnesium alloy WE43 developed by Esmaily et al. [53] was accomplished by SLM. The findings indicate that corrosion of prepared Mg alloys with SLM could be excellently improved once the effect of powder characteristics is more controlled and understood. In contrast to conventional construction techniques, Zumdick et al. [54] studied the characteristics of WE43 developed by SLM. The SLM samples had incredibly fine grains with the size of about 1 µm and uniform microstructure, and very delicate secondary stages, while the as-cast specimen had a grain size of 44.3 µm and various stages. Tensile testing of additively produced samples revealed an increased maximum tensile strength of 308 MPa and a 12 percent elongation to break. Further analysis of the WE43 compound developed by the SLM was performed by Qin et al to create porous Zn-xWE43 (x=0 percent, 2 percent, 5 percent, and 8 percent) substrates by SLM mechanically mixing WE43 and pure Zn powders. For the as-fabricated ZnWE43 substrates, elevated densification over 99.9 percent was recorded.

Using SLM, Chen et al. [55] developed double MgZn composites, and the mechanical and harmful properties were analyzed. With a mean range of 15µm, the SLM manufactured compound showed homogeneous grains. The precipitation of the MgZn phase and quick solidification have effectively prevented grain enlargement. Smaller grains decreased the speed of deterioration and increased the microhardness. Wei et al. [51] analyzed Mg-Zn binary composites with differing Zn proportions using the SLM technique. At Zn amount of 1 wt percent, almost full dense parts were acquired. The specimen of Mg-1Zn had comparable mechanical characteristics with that of the as-cast equivalents. Furthermore, pre-alloyed biomaterials consisting of Mg such as Mg–3 Zn and ZK60 were alloyed *in situ* throughout SLM using scarce elements of the earth (for example Nd [56] and Dy [52]) for increased sustainability and persistent coherence of biomaterials.

Mg-3Zn-xDy (x=0-5 w%) composites were produced by Long et al. [52] using the SLM technique. The speed of deterioration and hydrogen evolution of the Mg-3Zn-1Dy composite was greatly decreased due to the combined effect of smaller particle size, uniform microstructure, as well as the inclusion of the second step. Wu et al. produced Mg-Zn-Zr (ZK60) magnesium compound formulations. [57] by SLM. Experimental findings indicated that laser strength and speed of the scan played a key role in the efficiency determination of SLM ZK60.

SLM ZK60 with limited deficiencies and high structural precision could be achieved at a laser strength of 50 W and a scanning velocity of 500-800 mm/s. SLM ZK60 in Hanks' formulation has increased strength and corrosion stability, particularly as compared to cast ZK60. Thus, the developed SLM ZK60 holds great promise for biomedical applications due to its favorable mechanical characteristics and low degradable quality.

The in situ compounds of ZK60 with Cu [58] were found to have antibacterial properties and improved compressive strength in the main composite material. Shuai et al. [58] used the SLM technique to create the ZK60-Cu alloy, which has excellent antibacterial qualities and favorable corrosion in body fluid. The ZK60–0.4Cu compound has improved compressive strength attributable to grain accuracy improvement, dispersion bolstering, and precipitate boosting. The ZK60-Cu compound has a high level of cytocompatibility, according to experiments in cell culture. Another way to enhance the corrosion protection of MgZn alloys is to incorporate hydroxyapatite (HAp; $Ca_{10}(PO_4)_6(OH)_2$). [59, 60]. In this regard, Mg^{-3} Zn/xHAp blends were synthesized by Shuai et al.[61]

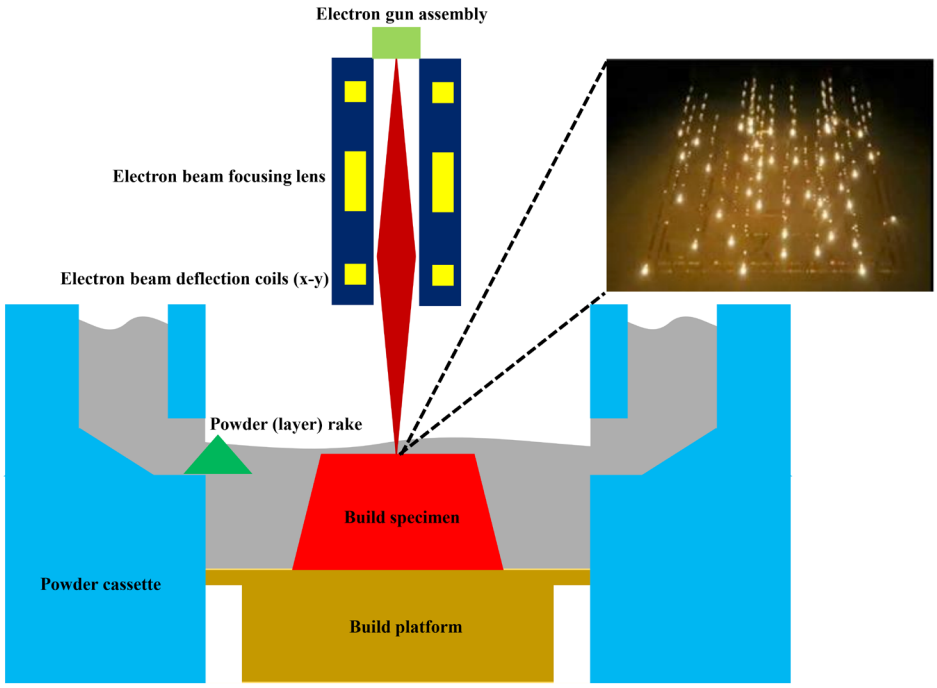

Fig. 3. Schematic illustration of an EBM system.

using the SLM technique. The relative density ranged from 95.5% to 97.9% for the as-built specimens. Fast solidification avoided HAp particle agglomeration and facilitated homogenous distribution. Increasing the amount of HAp contributed to the production of finer grains. Along with the development of the apatite coating sheet, finer grains contribute to increased resilience to biodegradation. Furthermore, by fine-grain reinforcement and second phase enhancement, the hardness of the Mg-3 Zn composite was strengthened.

Liu et al. [62] studied the SLM development of porous Mg-Ca alloys. Because of the grain refining and solid solution enhancement, the microhardness of the SLM-manufactured specimens was better than that of as-cast pure magnesium. Yao et al. [63] used SLM to change the surface of such Magnesium composites (Mg-Zn-Ca and Mg-Ca) to improve the corrosion effect and micro-hardness simultaneously. The corrosion ratio decreased and the microhardness increased in both Mg-0.5Zn-0.3Ca and Mg-0.6Ca. On the other hand, managing laser power density, and therefore avoiding the formation of unwanted pore spaces and unnecessary melting is challenging due to the widely divergent thermal characteristics of various components. Since certain additives have higher melting temperature, they cannot be fully melted and distributed, but they remain partially melted next to the matrix [64]. The grain size proportions of multi-material powders could be adjusted to account for variations in thermal properties, with a smaller size for a substance with a higher melting point [65].

Post-AM heating might be needed to enhance multi-material distribution and chemical property uniformity [50]. The availability of multi-material powders supply to the powder bed is also a critical factor in maintaining a consistent multi-material distribution within the resulting composite. Powder bed fusion is prone to strong thermal currents and may induce fractures and defects in the multi-material substrate since it uses large thermal powers. To allow successful application of laser power as well as other process parameters that should be synchronized with each material's physical characteristics and powder features, powder bed fusion for in situ versatile AM alloys or ceramic substrates necessitates robust and complicated enhancement. Furthermore, it is essential to consider the measures taken for the reuse and recycling of the remaining substances in the powder bed [66, 67].

3.2. Electron beam melting

EBM is another composite fabrication process that is expected to transform the implant- manufacturing sector. This device was developed and patented by Arc am AB, a Swedish company. The metal powder is liquefied using the energy of an electron stream [68]. The procedure is carried out in a vacuum chamber where the electron beam is the power supply. The vacuum by offering an atmosphere void of oxygen guarantees high purity and decreases the chance of picking up hydrogen. This function is highly helpful in the manufacture of titanium-6aluminium-4vanadium (Ti6Al4V) parts since it is possible to monitor the small amounts of interstitial components during manufacturing [69]. Besides, a high temperature of around 700 degrees Celsius is established in the system throughout the construction of the component to decrease excess tensions and thereby warpage and distortion [70].

Fig.3 shows the mechanism of the EBM process. The EBM device consists of a 60 kW electron gun that produces a guided energy intensity beam over 100 kW/cm2 (equivalent to an electron beam-welding unit or electron gun in a scanning electron microscope). Electromagnetic lenses control the beam concentration, and deflection coils direct the beam's motion on the building table. A powder layer with a thickness of 100 m is dispersed over the table to make a part. Two hoppers placed within the construction chamber supply the powder. From both ends, a running rake brings in powder and spreads it across the table. During EBM, initially, the electron beam heat up the powder layer with faster scanning, accompanied by powder layer melting according to the CAD model's geometry. Each layer of a component is built in two phases. The outer boundary of the part is first built, known as contouring, and then the powder inside the contour begins to melt, forming a single sheet. [71, 72].

EBM was employed to manufacture orthopedic parts including jaw, hip, knee, substitutes, and maxillofacial plates [73]. This procedure continues until the required three-dimensional portion is entirely completed The implants developed by EBM, such as acetabular cups, have also been approved by the Food and Drug Administration (FDA) of the United States and have been CE accredited since 2010 and 2007, respectively [74, 75]. Both of these procedures share common benefits and are actively taken into account in the manufacturing of orthopedic implants.

These benefits include complex product processing, innovative designs, hollow systems, and products with practical gradients. A cost-effective strategy that causes lowering manufacturing costs and shortening the period to market for high-value products. Some of the benefits include superior structural properties, virtually no porosity, the ability to mix different components, reduced material waste dramatically. Exclusion of costly instrumentation. Because of these benefits, various scholars have performed multiple studies to confirm the merit of these methods in implant production. As an artificial bone that is implanted inside the corpus, orthopedic implants are often used for structural strengthening. Temporary implants, including screws and plates, as well as permanent implants, can be utilized to repair body sections such as fingers, knees, and hips. [76, 77]. Permanent implants rely more on resilience, durability, and tolerance to corrosion in joint replacements and tribology.

A study of the Magnesium alloy AZ91HP processed using High Current Pulsed Electron Beam (electron energy of 30 keV, a pulse length of 1 μs, and energy density of 3 J/cm^2) has been reported by Gao et al. [78] After treatment, as demonstrated by sliding pressure, corrosion, and immersion tests, the wear and corrosion tolerance of the alloy was substantially increased. Schmid et al. [79] developed AZ91 Mg alloy using the EBM process. While treating magnesium under typical laser beam melting conditions, the findings revealed keyhole melting happens, and modifying energy input by changing the layer thickness has a lesser influence than changing the distance of the hatch, scan rate, or laser strength.

4. Characteristics of Mg alloy and composite implants produced by AM

4.1. Mechanical properties

Implants must be immune to anatomical loads. Thus, mechanical properties including stiffness, tensile and compressive strength, hardness flexibility, durability, and ductility must be evaluated prior to therapeutic implementation. [80]. The alleged stress shielding, that happens when the external pressures are acting upon the implant instead of bone, results in a substantial discrepancy between the elastic moduli of the body tissue and implant. Stress shielding induces bone necrosis that leads to the implant/scaffold destabilization and ultimately the implant/premature scaffold collapse. The cancellous and cortical bones have an elastic modulus in the range of 22.4 to 132.3 MPa and 7.7 to 21.8 GPa, respectively. An elastic modulus imitating the normal human bone elastic modulus [81, 82] should be demonstrated by implants. Adapting the elastic modulus to the proper rate is also vital for the nature of the implant.Accordingly, multiple methods could be used to avoid the implant/scaffold and bone from mismatching mechanical characteristics. Mixing with β stabilizers is one method for reducing the elastic moduli of the implant by applying a β step in the structure. Together with porosity, elastic moduli also can be efficiently decreased [83-85].

Based on Gibson and Ashby model [86], relative density is the most significant design feature of a porous structure that affects Young's module. The ratio of the density of the elastic substance (ρ) to the density of the solid material (ρ_s) is known as relative density. The given formulas describe the relations between the elastic modulus, plastic failure strength, and relative density [20]:

$$\sigma_{pl} = 0.3\left(\rho / \rho_s\right)^{1.5} \rho_{ys} \tag{1}$$

$$E = \rho(\rho_s)^2 E_s \tag{2}$$

Where σ_{pl} is the intensity of the plastic failure, ρ/ρ_s the relative density, the yield strength is ρ_{ys}. E is Young's modulus; the subscript (s) reflects the substrate material features. Provided formulas show that increasing porosity reduces the elastic modulus' strength and causes plastic breakdown. However, by grain refining as per the Hall-Petch model, the mechanical properties of an implant/scaffold can be increased as follows [87]:

$$\sigma_y = \sigma_0 + \frac{k}{\sqrt{d}} \tag{3}$$

Here yield stress is σ_y, σ_0 is a material constant for the starting stress for dislocation movement, k is a material constant known as strengthening coefficient, and d denotes the size of the grain. In a related way as reported by the Hall-Petch equation, grain refining greatly increases the hardness of the products according to Eq. 4 [87];

$$H = H_0 + \frac{k}{\sqrt{d}} \tag{4}$$

Where H is the material hardness, H_0 and k are suitable constants correlated with the material hardness, and d is the particle size.

As earlier described, SLM-manufactured composites retain refined grains because of quick cooling and solidification. Researchers examined the processing of biodegradable Magnesium composites of different compositions using SLM.

Sing et al. [88] reported multi-material production in SLM employing AlSi10Mg and UNS C18400 copper alloy. Under a three-point bending examination, the tensile strength of Cu at the root was determined to be 176 ±31 MPa, and the flexural strength of Al at the root was assessed about 200 MPa for Cu and 500 MPa for Al.

According to the Hall-Petch formula, a single track of pure Magnesium demonstrated grain sophistication and increased hardness in the study by Ng et al. [40]. Yang et al. [44] used the SLM technique to create pure Magnesium cubes, which was then verified by them. SLM then produced a variety of Mg alloys with increased toughness cause of the high cooling and solidification speeds [62]. The yield strength, elastic modulus, compressive strength, and tensile strength of the SLM-generated Magnesium models outperformed widely manufactured equivalents and they were favored for orthopedic applications. Research work shows that in compliance with the Hall-Petch model, grain refining increases the hardness of the biodegradable Mg sections. The hardness of the Mg generated by the SLM varied from 0.4 to 1.2 GPa [89].

Mg-Zn dual composites with seven varied formulas (Zn = 1, 2, 4, 6, 8, 10, and 12 wt%) were produced by Wei et al. [51] by employing SLM. The hardness and tensile measurements revealed that with the as-cast equivalent, only the Mg-1Zn sample had equivalent mechanical properties. Mechanical characteristics of the SLM-processed alloys were substantially weakened at higher Zn content primarily due to the decline in the level of densification. In addition, Qin et al. [90] manufactured AM Zn-xWE43 porous scaffolds containing various WE43 volume ratios. Zn-5WE43 had the maximum tensile strength of 335.4 MPa, but the elongation was just 1%. The compressive strength and Young's modulus of Zn-5WE43 porous substrates were 73.2 MPa and 2480 MPa, respectively, while pure Zn porous substrates were 22.9 MPa and 950 MPa. Li et al. [91] developed geometrically organized porous Mg (WE43) substrates through the SLM process based upon the diamond unit cell. Substrates were constructed to yield 67 percent porosity with a pore size of 600 μm and strut size of 400 μm, whereas the scaffolds that have already been developed had an approximate 64 percent porosity and strut size of 420 μm. The mechanical properties of the porous WE43 (E=0.7–0.8 GPa) substrates were also found to remain within the limit reported for trabecular bone (E=0.5–20 GPa) after 4 weeks of biodegradation. The modeled configuration accurately aligned the real topology of the porous architectures, which included a completely entangled porous construct, elevated porosity, and explicitly regulated geometry of the unit cells. A

desirable biodegradation activity was demonstrated by additively produced porous Mg samples with around 20 percent volume reduction after 4 weeks. Small cytotoxicity was registered at less than 25 percent.

4.2. Biodegradability behavior

The Mg-based substances are recommended for medical applications due to their biodegradability. The objective of biodegradable Mg is to establish a functional interaction in vitro and in vivo involving biodegradable specimens of magnesium and the natural biological setting while traditional metals are utilized as biocompatible substances to enhance mechanical characteristics, decrease production costs, and improving corrosion resistance [92]. Different studies have been conducted regarding the cellular mechanisms and biological environment-biomaterial interaction to emphasize the biological effect of corrosion byproducts[93, 94]. Many research groups have focused on Mg to develop new medical applications, particularly after it was discovered that implanting magnesium tools causes no noticeable alterations in blood content. [95-97].

Because of the increased content of grain borders, grain refining potentially accelerates the amount of corrosion. Gollapudi et al. defined the effect of particle sizes on the corrosion rate [98] as given in Eq. 5:

$$i_{corr} = A + B(d)^{1/2} \exp\left(-9/8S_n^2\right) \quad (5)$$

The corrosion current is i_{corr}, *A,* and *B* are constants that depend on the impurity level or material composition, the grain size distribution is S_n and the mean grain size is d in this equation.

Many corrosion materials have a significant influence on the rate of corrosion of biodegradable metals [99, 100]. Fine-grain, because of the formation of corrosion products can lead to a decrease in the rate of corrosion in a passivated environment. According to various studies, the corrosion rate of magnesium and its composites declines as grain size reduces [89]. The manufacturing process, architecture, and material selected all affect the biodegradation efficiency of additively processed magnesium. In addition, the condition of processing has a prevailing influence on the as-built parts' biodegradation characteristics. Niu et al. [101] studied the bulk pure magnesium's corrosion behavior, which was prepared by the SLM method. The results of the study highlighted the significance of selecting proper parameters for the magnesium SLM processing to minimize corrosion rate and processing pores. The rate of corrosion (r) is calculated by the following equation:

$$r = (M_1 - M_2)/t_i \quad (6)$$

In this equation, M_1 is the material mass before corrosion and M_2 is the material mass after corrosion, and t_i is the immersion time. Researches exhibit that the corrosion rate of magnesium alloys can be decreased by grain refinement [102]. As noted, the SLM process involves fast cooling causes homogenized microstructure formation and fine grains leading to the improvement in corrosion resistance [103]. Li et al. [91] prepared WE43 scaffolds by the SLM method. The as-fabricated scaffolds showed improved biodegradation resistance of 0.17 ml/cm^2·day compared with the as-extruded and as-cast counterparts of 0.3 ml/cm^2·day. Xie et al. [104] investigated SLMed Mg-xMn with various content of Mn. The XPS spectra of the corrosion surface exhibited that alloying manganese into magnesium by SLM produced a protective film of manganese oxide, which reduced the biodegradation rate. All the results of the corrosion surface morphologies, immersion test, and electrochemistry test coincided well. The SLMed Mg-0.8Mn had the lowest rate of biodegradation. When manganese content was more than 0.8 wt.%, the effect of the undissolved manganese phase on the reduction of the biodegradation resistance counteracted the effect of the relatively protective layer of manganese oxide on the enhancement of the biodegradation resistance.

The corrosive behavior of pure Fe and AM WE43-based porous scaffolds was investigated by Li et al. [91]. The corrosive behavior was studied in SBF for 7 days and the results showed that the weight losses of AM porous WE43 and the bulk WE43 plates (10×10×2 mm^3) were almost 9% and 5%, respectively. The process of SLM was used by Shuai et al. [105] to promote the ZK60 corrosion resistance for potential applications as biodegradable implants. The extended solid solution, homogenized microstructure, and grain refinement improved ZK60 alloy corrosion resistance because of the fast grain refinement in the SLM process. Nd was incorporated into ZK60 alloy with the SLM process by Shuai et al. [56]. The as-prepared sample had intermetallic phases and fine grains of α-Mg along the grain boundaries. The resistance to degradation increased with the dense surface layer formation promoted by the Nd_2O_3, besides the structure of the 3D honeycomb of intermetallic phases resulted in the formation of a tight barrier for corrosion prevention.

Rakesh et al. [106] studied Mg-1Zn-2Dy alloy by SLM and their results exhibited that the surface energy was changed with LSM because of changes in the chemical composition, microstructure, and surface morphology of the material. The detailed degradation research was performed in Hank's balanced salt solution (HBSS). The enhancement in the degradation behavior followed by laser surface melting is attributed to the microstructural refinement because of the fast cooling and heating of the melted zone. Besides the grain size, an essential factor is the intermetallic phase, which affects the Mg alloy's biodegradation behavior [107]. Shuai et al. [108] investigated various intermetallic phase volume fractions and grain size by adding different concentrations of Al into Mg–Zn alloy. In this experiment, ZK30-xAl cubes with the dimensions of 5 mm×5 mm×5 mm were prepared using the SLM method. Based on the results, with an increase in the content of Al, the refinement of the grain size occurred and the volume fraction of intermetallic phase was reduced. When the Al content was lower than 3 wt%, the main factor that affected the degradation performance was the grain refinement. Many grain boundaries were generated by the finer grains causing readily passivation of the alloy leading to an enhanced resistance to degradation. Nevertheless, by increasing the content of Al, the major factor affecting the degradation behavior was the intermetallic phase even though the size of grain was more refined.

In another work conducted by Yang et al. [109], mesoporous SiO_2 was incorporated into ZK60 alloy for the enhancement of the degradation resistance using SLM. Since the rapid cooling and heating occur in SLM, mesoporous silica particles homogeneously dispersed in the magnesium matrix and led to the formation of a decent interface binding. Mesoporous SiO_2 can be used for magnesium surface passivation because of its positive corrosion potential. Besides, the exceptional bioactivity and mesoporous structure of SiO_2 promoted the apatite layer deposition, which has a role as a protection film against corrosion of the Mg matrix. Table 1 summarizes previously studied work regarding the biodegradation behavior of magnesium prepared by AM. Improved biodegradation resistance is achieved by the improved microstructure resulting in the rapid cooling and fast solidification involved in the SLM process.

4.3. Biocompatibility

The chemical composition and degradation products mostly specify the biocompatibility of biodegradable metal-based implants. Therefore, the strict usage of biocompatible powders should be the main attention. The information gathered from the biodegradable bulk material design can help with the primary design of powder composition [89, 110-112]. For the enhancement of biocompatibility and mechanical integrity of bulk magnesium alloys during biodegradation, surface biofunctionalization has been carried out [113].

Desirable results have been obtained for biodegradable magnesium

Table 1.
Properties of biodegradable Mg manufactured by AM

Material	AM method	Mechanical performance	Biodegradation behavior	Biocompatibility	Reference
TiTa	SLM	Elastic modulus of ~75 GPa and tensile strength of ~924 MPa	Corrosion resistance	In contrast to other SLM titanium alloys, this alloy is highly biocompatible and has no toxic materials like aluminum or vanadium.	Sing et al. [64]
WE43	L-PBF	With the increase of the strut diameter from 275 μm to 800 μm, the increase in the elastic modulus was from 0.2 to 0.8 GPa, and also the yield strength was improved from 8 to 40 MPa.	The solution treated and as-printed scaffolds showed the lowest rate of corrosion of 2–3 mm/year and the corrosion rate could be decreased to ~0.1 mm/year with plasma electrolytic oxidation surface treatments.	Scaffolds based on WE43 magnesium alloy with the PEO surface treatment presented acceptable biocompatibility.	Li et al. [127]
SLM-prepared ZK60 and cast ZK60	SLM	The hardness of cast and SLM ZK60 was 0.78 and 0.55 GPa, respectively, while their elastic moduli were similar.	Higher corrosion resistance in Hanks' solution was exhibited by SLM ZK60 compared to cast ZK60 so that the corrosion current density and hydrogen evolution rate reductions were 50 % and 30 %, respectively.	-	Wu et al. [57]
ZK60/BG	LPBF	Mechanical properties were improved due to the refined grains in which reinforcing particles were orderly dispersed.	LPBF with a fast process of solidification resulted in a homogenized and refined microstructure. This feature was also considered responsible for the improved corrosion resistance of ZK60/BG.	ZK60/BG with improved biocompatibility promoted differentiation and cell growth, which led to accelerating healing of bones as an in vivo implant.	Yang et al. [9]
Fe-Mg	SLM	-	After immersion for 21 days the rate of degradation improved by 2.74 times.	The MG-63 cells proliferated faster, showing excellent cytocompatibility.	Shuai et al. [128]
Mg-Ca and Mg-Zn-Ca	SLM	The improvement of microhardness (HV0.1(for Mg–0.6Ca and Mg–0.5Zn–0.3Ca was from 46 ± 1 HV to 56 ± 1 HV and from 47 ± 3 HV to 55 ± 3 HV, respectively.	The rate of corrosion for laser-processed Mg–0.5Zn–0.3Ca and the laser-processed Mg–0.6Ca reduced from 1.6 ± 0.1 mm/y to 0.7 ± 0.2 mm/y and from 2.1 ± 0.2 mm/y to 1.0 ± 0.1 mm/y, respectively.	The laser processed magnesium alloys showed excellent biocompatibility.	Yao et al. [63]
Ti+Mg	Inkjet 3D printing	Composite of Ti+Mg showed high UCS (418MPa) and low modulus (5.2GPa) matching bone.	After 5 days of immersion, porous Ti showed a poor corrosion rate of ~1.14 μm/year, while Ti + Mg composites exhibited a corrosion rate of <1 mm/year.	The results of cell viability showed the absence of mild cytotoxicity improved the proliferation rate of SAOS-2 osteoblastic bone cells.	Meenashisundaram et al. [129]
AZ31B-HA composites	Friction stir AM	-	Corrosion resistance was higher in the composites compared to untreated AZ31B because of an optimum balance between positive influences of grain size refinement and the limited number of local galvanic couples.	-	Ho et al. [130]
ZK30-xCu	SLM	-	Biodegradation rate order was as follows: ZK30 < ZK30-0.1Cu < ZK30-0.2Cu < ZK30-0.3Cu	The alloys show good cytocompatibility and antibacterial ability.	Xu et al. [45]
Mg-5.9Zn-0.13Zr	3D printing	With sintering process conducted at 573 °C and holding time up to 60 h, comparable elastic modulus, compressive properties, and density, close to that of human cortical bone were obtained.	-	-	Salehi et al. [131]
AZ61	SLM	The ultimate tensile strength of the as-synthesized alloy was measured to be 93% higher compared to the as-cast alloy, the increase in the yield strength was 136%, and the decrease in the surface roughness was from 18.95 to 7.49 μm.	-	-	Liu et al. [132]
WE43	L-PBF	-	It can be shown that, because of high process-induced surface roughness, which supports corrosion of locally intensified, several crack initiation sites are appearing, which is one of the major reasons for the intense decrease in fatigue strength.	-	Wegner et al. [133]

Table 1. (Continued)

Material	AM method	Mechanical performance	Biodegradation behavior	Biocompatibility	Reference
Zn-xWE43	L-PBF	The highest tensile strength was 335.4 MPa relating to Zn-5WE43, while the elongation was only 1%. Young's modulus and compressive strength of Zn-5WE43 porous scaffolds were 2480 MPa and 73.2 MPa, respectively, but for pure Zn porous scaffolds, these values accounted for 950 MPa and 22.9 MPa respectively.	The powders of Zn-Mg alloy based exhibited hopeful prospects for applications of biodegradable.	-	Qin et al. [90]
ZK30/BG composites	SLM	-	The rate of degradation of the ZK30 matrix declined with the BG introduction.	Cytocompatibility was enhanced with the BG addition.	Yin et al. [122]
ZK60-xCu	SLM	Because of the refinement of the grains and uniform dispersion of MgZnCu phases with short-bar shapes, the compressive strength improved.	ZK60-Cu alloys show an excellent biodegradation rate.	ZK60-Cu alloys showed good cytocompatibility and strong antibacterial ability.	Shuai et al. [58]

alloys having different compositions. When the content and type of the alloying element(s) are selected carefully, the biodegradation resistance of magnesium can be remarkably increased without scarifying its mechanical function as well as its biocompatibility. The in vivo and in vitro tests have many differences. Sanchez et al. [114] reported the lower rate of corrosion (1-4 times) for magnesium alloys in the in vivo test in comparison with the in vitro test. Some of the results are attributed to the in vivo evaluations of vascular stents based on biodegradable metals [115]. In addition, in microstructure and chemical composition, the biocompatibility results are attributed to time, implantation position together with structure design [89, 116]. The potential of using pure magnesium-based screws to fix vascularized bone graft in ONFH patients was studied by Zhao et al. [31]. The results showed the biocompatibility of the magnesium screw and its efficiency in bone flap stabilization. Its degradation rate was comparable to the tissue-healing rate; also, the released magnesium ions could stimulate the formation of new bone.

$Mg_3(PO_4)_2$ is a bioceramic exhibiting special bioactivity, biodegradability, and biocompatibility [20]. A composite scaffold based on gelatin/$Mg_3(PO_4)_2$ with binder jetting was fabricated by Farag and Yun [117]. Dense struts were formed by the addition of gelatin into $Mg_3(PO_4)_2$ up to 6 wt%; therefore, it considerably enhanced the mechanical performance of the scaffolds. In addition, the composite scaffolds showed good cell affinity and wettability. Binder jetting was also used on $Mg_3(PO_4)_2$ powder by Vorndran et al. [118]. The binder liquid used in this study composed of K_2HPO_4 (2 M), 20% H_3PO_4 or $(NH_4)_2HPO_4$ (0.5 M) for the formation of a matrix of, newberyite ($MgHPO_4 \cdot 3H_2O$), struvite-(K) ($MgKPO_4 \cdot 6H_2O$), or struvite ($MgNH_4PO_4 \cdot 6H_2O$) by employing a hydraulic setting reaction.

In order to inhibit infections inside the human body, it is essential to incorporate antibacterial properties into implants. As *in vitro* studies show, antibacterial features are not presented by Mg metal and alloys [58]. By coupling 3D printed and traditionally manufactured Mg alloys with Cu, bacterial activity decreased. However, traditional methods of manufacturing cannot deliver Mg-Cu components with good quality due to galvanic corrosion issues. For low levels of Cu in Mg alloys that are below the limit of solid solubility, additive manufacturing has been shown to be able to handle this challenge [45]. Studies show that after 72 h under normal pH conditions, *Escherichia Coli* colony count was reduced to zero by the addition of 0.4 wt% Cu powder to ZK60. Moreover, blending bioactive glass with Mg-based alloys has demonstrated the enhancement of cytocompatibility [119, 120]. Besides, resistance to degradation in the ZK30 Mg alloy was found to be improved in simulated body fluid by the increase in the bioactive glass content in the ZK30 powder mixture. This is due to magnesium ion release limitations within the body. Using laser additive manufacturing, Yang et al. [9] reinforced Mg with bioglass. To compare the biocompatibility of the composite with ZK60 as control, the as-prepared part acquired at a volumetric energy density of 185.19 J/mm^3 was used. Generally, observed dead cells were very few. Briefly, improved biocompatibility provided by ZK60/BG enhanced differentiation and cell growth leading to accelerated bone healing.

Mg–Y–RE–Zr alloy prepared by conventional methods has been stated to exhibit good osteoconductivity and biocompatibility and no toxicity [121]. This alloy is being used for the fabrication of screws to treat hallux valgus and bone fractures in the European Union. Y is an important alloying element, which enhances the overall behavior of the alloy and its degradation because this element decreases galvanic coupling due to the formation of intermetallic phases. It also produces a net improvement in the corrosion resistance by protective surface oxide layer formation, depending on the environment [122]. Bär et al. [121] created implants made of WE43 by additive manufacturing. The results demonstrated that the sample has good osteoconductivity and biocompatibility. Yao et al. [63] studied the SLM magnesium alloys such as Mg–0.5Zn–0.3Ca and Mg–0.6Ca and according to the results good biocompatibility was found in laser processed magnesium alloys. In addition, the enhanced properties are related to the modified surface chemistry, residual stress, confined impurity elements, and laser-induced grain refinement. The dual alloying influence of manganese and/or Sn on the performance of magnesium alloys prepared by SLM was investigated by Gao et al. [123]. The alloys of Mn- and/or Sn-containing exhibited good cytocompatibility as indicated by increased viability of MG-63 cells and the normal morphology revealing that the developed alloy of AZ61-Mn-Sn is a promising choice for biodegradable bone implants. Table 1 exhibits the biocompatibility, biodegradation, and mechanical properties of different materials produced by AM.

5. Conclusions and future insights

Mg-based implants with personalized designs consistent with the patient's anatomic data can be created using additive manufacturing. Although the probability of sacrificial material elimination has been exhibited by recent studies, as-prepared magnesium components still lack sufficient formation quality. EBM seems to be inappropriate because severe evaporation of magnesium affects the propagation of electron beam in the vacuum environment within the build chamber. In the SLM process, high densification is achieved because of the efficient infiltration as well as complete melting of magnesium resulting in the elimination of voids in the bulk struts/material. The fast solidification and high rates of cooling in the SLM process are favored to obtain improved microstructure with an enhanced solid solution, homogenized phase distribution,

and refined grains. Therefore, the corrosive and mechanical properties of magnesium produced by SLM are superior to their traditionally produced counterparts. Powder properties and processing conditions notably affect the mechanical and biological performance of the as-prepared magnesium implants and scaffolds, microstructure, dimensional accuracy, and formation quality. The optimal processing conditions and powder properties led to higher energy efficiency and material densification. The topology of scaffolds notably influences differentiation, proliferation, and new cells' attachment. Studies concentrating on the manufacturing of Mg with various lattice structures by the AM process are quite limited.

It is required to conduct more studies for comparative investigation regarding the influence of pore porosity, topology, and various lattice structures, to recognize the ideal design for scaffolds to render the best performance. There might be some differences in the biological properties of the as-prepared magnesium in vivo and in vitro. There are wide in vitro studies to evaluate the biodegradation characteristics of additively manufactured Mg alloys, however, limited reports are focusing on the in vivo performance of these alloys. Therefore, it is recommended to carry out more in vivo investigations to shed light on the biodegradation performance of magnesium implants manufactured by AM. Eventually, based on the period required for the healing of the defected tissues, the in vivo performance of additively manufactured magnesium implants in terms of time (up to ~2 months) is needed to be investigated to ultimately succeed of the implants in clinical applications.

Acknowledgments

The authors received no financial support for the research, authorship and/or publication of this article.

Conflict of interest

The authors declare that there is no conflict of interest.

REFERENCES

[1] I. Antoniac, D. Popescu, A. Zapciu, A. Antoniac, F. Miculescu, H. Moldovan, Magnesium filled polylactic acid (PLA) material for filament based 3D printing, Materials 12(5) (2019) 719.

[2] T.Y. Kwak, J.Y. Yang, Y.B. Heo, S.J. Kim, S.Y. Kwon, W.J. Kim, D.H. Lim, Additive manufacturing of a porous titanium layer structure Ti on a Co–Cr alloy for manufacturing cementless implants, Journal of Materials Research and Technology 10 (2021) 250-267.

[3] J.B. Hochman, J. Kraut, K. Kazmerik, B.J. Unger, Generation of a 3D printed temporal bone model with internal fidelity and validation of the mechanical construct, Otolaryngology–Head and Neck Surgery 150(3) (2014) 448-454.

[4] E.K. O'Brien, D.B. Wayne, K.A. Barsness, W.C. McGaghie, J.H. Barsuk, Use of 3D printing for medical education models in transplantation medicine: a critical review, Current Transplantation Reports 3(1) (2016) 109-119.

[5] D. Popescu, D. Laptoiu, Rapid prototyping for patient-specific surgical orthopaedics guides: A systematic literature review, Proceedings of the Institution of Mechanical Engineers, Part H: Journal of Engineering in Medicine 230(6) (2016) 495-515.

[6] D. Popescu, D. Laptoiu, R. Marinescu, I. Botezatu, Design and 3D printing customized guides for orthopaedic surgery–lessons learned, Rapid Prototyping Journal 24(5) (2018) 901-913.

[7] S.L. Sing, J. An, W.Y. Yeong, F.E. Wiria, Laser and electron-beam powder-bed additive manufacturing of metallic implants: A review on processes, materials and designs, Journal of Orthopaedic Research 34(3) (2016) 369-385.

[8] A. Masoudian, A. Tahaei, A. Shakiba, F. Sharifianjazi, J.A. Mohandesi, Microstructure and mechanical properties of friction stir weld of dissimilar AZ31-O magnesium alloy to 6061-T6 aluminum alloy, Transactions of nonferrous metals society of China 24(5) (2014) 1317-1322.

[9] Y. Yang, C. Lu, S. Peng, L. Shen, D. Wang, F. Qi, C. Shuai, Laser additive manufacturing of Mg-based composite with improved degradation behaviour, Virtual and Physical Prototyping 15(3) (2020) 273-293.

[10] C. Wu, W. Zai, H. Man, Additive manufacturing of ZK60 magnesium alloy by selective laser melting: Parameter optimization, microstructure and biodegradability, Materials Today Communications 26 (2020) 101922.

[11] D. Carluccio, C. Xu, J. Venezuela, Y. Cao, D. Kent, M. Bermingham, A.G. Demir, B. Previtali, Q. Ye, M. Dargusch, Additively manufactured iron-manganese for biodegradable porous load-bearing bone scaffold applications, Acta biomaterialia 103 (2020) 346-360.

[12] V.S. Telang, R. Pemmada, V. Thomas, S. Ramakrishna, P. Tandon, H.S. Nanda, Harnessing Additive Manufacturing for Magnesium Based Metallic Bioimplants: Recent Advances and Future Perspectives, Current Opinion in Biomedical Engineering 17 (2021) 100264.

[13] R. Karunakaran, S. Ortgies, A. Tamayol, F. Bobaru, M.P. Sealy, Additive manufacturing of magnesium alloys, Bioactive Materials 5(1) (2020) 44-54.

[14] M.N. Jahangir, M.A.H. Mamun, M.P. Sealy, A review of additive manufacturing of magnesium alloys, AIP Conference Proceedings, AIP Publishing LLC 1980(1) (2018) 030026.

[15] T. Trang, J. Zhang, J. Kim, A. Zargaran, J. Hwang, B.-C. Suh, N. Kim, Designing a magnesium alloy with high strength and high formability, Nature communications 9(1) (2018) 1-6.

[16] A. Dehghanghadikolaei, H. Ibrahim, A. Amerinatanzi, M. Elahinia, Biodegradable magnesium alloys, Metals for Biomedical Devices, Second ed., Elsevier, Netherlands, 2019, pp. 265-289.

[17] A. Moghanian, A. Ghorbanoghli, M. Kazem-Rostami, A. Pazhouheshgar, E. Salari, M. Saghafi Yazdi, T. Alimardani, H. Jahani, F. Sharifian Jazi, M. Tahriri, Novel antibacterial Cu/Mg-substituted 58S-bioglass: Synthesis, characterization and investigation of in vitro bioactivity, International Journal of Applied Glass Science 11(4) (2020) 685-698.

[18] B.R. Powell, P.E. Krajewski, A.A. Luo, Chapter 4 - Magnesium alloys for lightweight powertrains and automotive structures, in: P.K. Mallick (Ed.), Materials, Design and Manufacturing for Lightweight Vehicles (Second Edition), Woodhead Publishing, United Kingdom, 2021, pp. 125-186.

[19] A. Sheikhani, R. Roumina, R. Mahmudi, Hot deformation behavior of an extruded AZ31 alloy doped with rare-earth elements, Journal of Alloys and Compounds 852 (2021) 156961.

[20] N. Sezer, Z. Evis, M. Koç, Additive manufacturing of biodegradable magnesium implants and scaffolds: Review of the recent advances and research trends, Journal of Magnesium and Alloys 9(2) (2021) 392-415.

[21] Y. Luan, P. Mao, L. Tan, J. Sun, M. Gao, Z. Ma, Optimising the mechanical properties and corrosion resistance of biodegradable Mg-2Zn-0.5Nd alloy by solution treatment, Materials Technology 37(8) (2021) 663-672.

[22] J. Huang, Y. Ren, Y. Jiang, B. Zhang, K. Yang, In vivo study of degradable magnesium and magnesium alloy as bone implant, Frontiers of Materials Science in China 1(4) (2007) 405-409.

[23] C. Hampp, B. Ullmann, J. Reifenrath, N. Angrisani, D. Dziuba, D. Bormann, J.M. Seitz, A. Meyer-Lindenberg, Research on the biocompatibility of the new magnesium alloy LANd442—an in vivo study in the rabbit tibia over 26 weeks, Advanced Engineering Materials 14(3) (2012) B28-B37.

[24] J. Dai, Z. Liu, B. Yu, Q. Ruan, P.K. Chu, Effects of Ti, Ni, and Dual Ti/Ni Plasma Immersion Ion Implantation on the Corrosion and Wear Properties of Magnesium Alloy, Coatings 10(4) (2020) 313.

[25] Y. Li, C. Wen, D. Mushahary, R. Sravanthi, N. Harishankar, G. Pande, P. Hodgson, Mg–Zr–Sr alloys as biodegradable implant materials, Acta biomaterialia 8(8) (2012) 3177-3188.

[26] Z. Li, X. Gu, S. Lou, Y. Zheng, The development of binary Mg–Ca alloys for use as biodegradable materials within bone, Biomaterials 29(10) (2008) 1329-1344.

[27] H.R.B. Rad, M.H. Idris, M.R.A. Kadir, S. Farahany, Microstructure analysis and corrosion behavior of biodegradable Mg–Ca implant alloys, Materials & Design 33 (2012) 88-97.

[28] A. Ghanbari, H. Jafari, F.A. Ghasemi, Wear Behavior of Biodegradable Mg–5Zn–1Y–(0–1) Ca Magnesium Alloy in Simulated Body Fluid, Metals and Materials International 26(3) (2020) 395-407.

[29] S. Wang, X. Zhang, J. Li, C. Liu, S. Guan, Investigation of Mg–Zn–Y–Nd alloy for potential application of biodegradable esophageal stent material, Bioactive Materials 5(1) (2020) 1-8.

[30] M. Liu, J. Wang, S. Zhu, Y. Zhang, Y. Sun, L. Wang, S. Guan, Corrosion fatigue of the extruded Mg–Zn–Y–Nd alloy in simulated body fluid, Journal of Magnesium and Alloys 8(1) (2020) 231-240.

[31] D. Zhao, S. Huang, F. Lu, B. Wang, L. Yang, L. Qin, K. Yang, Y. Li, W. Li, W. Wang, Vascularized bone grafting fixed by biodegradable magnesium screw for treating osteonecrosis of the femoral head, Biomaterials 81 (2016) 84-92.

[32] F. Sharifianjazi, A. Esmaeilkhanian, M. Moradi, A. Pakseresht, M.S. Asl, H. Karimi-Maleh, H.W. Jang, M. Shokouhimehr, R.S. Varma, Biocompatibility and mechanical properties of pigeon bone waste extracted natural nano-hydroxyapa-

tite for bone tissue engineering, Materials Science and Engineering: B 264 (2021) 114950.
[33] J. Wu, B. Lee, P. Saha, P. N Kumta, A feasibility study of biodegradable magnesium-aluminum-zinc-calcium-manganese (AZXM) alloys for tracheal stent application, Journal of Biomaterials Applications 33(8) (2019) 1080-1093.
[34] X. Wei, P. Liu, S. Ma, Z. Li, X. Peng, R. Deng, Q. Zhao, Improvement on corrosion resistance and biocompability of ZK60 magnesium alloy by carboxyl ion implantation, Corrosion Science 173 (2020) 108729.
[35] I. Gibson, D. Rosen, B. Stucker, M. Khorasani, Design for Additive Manufacturing, in: I. Gibson, D. Rosen, B. Stucker, M. Khorasani (Eds.), Additive Manufacturing Technologies, Springer International Publishing, Cham, 2021, pp. 555-607.
[36] Z. Wang, W. Wu, G. Qian, L. Sun, X. Li, J.A. Correia, In-situ SEM investigation on fatigue behaviors of additive manufactured Al-Si10-Mg alloy at elevated temperature, Engineering Fracture Mechanics 214 (2019) 149-163.
[37] H. Rezaeifar, M.A. Elbestawi, On-line melt pool temperature control in L-PBF additive manufacturing, The International Journal of Advanced Manufacturing Technology 112(9) (2021) 2789-2804.
[38] S.Y. Choy, C.-N. Sun, W.J. Sin, K.F. Leong, P.-C. Su, J. Wei, P. Wang, Superior energy absorption of continuously graded microlattices by electron beam additive manufacturing, Virtual and Physical Prototyping 16(1) (2021) 14-28.
[39] C. Ng, M. Savalani, H. Man, I. Gibson, Layer manufacturing of magnesium and its alloy structures for future applications, Virtual and physical prototyping 5(1) (2010) 13-19.
[40] C. Ng, M. Savalani, M. Lau, H. Man, Microstructure and mechanical properties of selective laser melted magnesium, Applied Surface Science 257(17) (2011) 7447-7454.
[41] L. Thijs, F. Verhaeghe, T. Craeghs, J. Van Humbeeck, J.-P. Kruth, A study of the microstructural evolution during selective laser melting of Ti–6Al–4V, Acta materialia 58(9) (2010) 3303-3312.
[42] H. Rotaru, R. Schumacher, S.-G. Kim, C. Dinu, Selective laser melted titanium implants: a new technique for the reconstruction of extensive zygomatic complex defects, Maxillofacial plastic and reconstructive surgery 37(1) (2015) 1.
[43] S. Merkt, A. Kleyer, A.J. Hueber, The Additive Manufacture of Patient-tailored Finger Implants: Feasibility study: implants based on XtremeCT technique, Laser Technik Journal 11(2) (2014) 54-56.
[44] Y. Yang, P. Wu, X. Lin, Y. Liu, H. Bian, Y. Zhou, C. Gao, C. Shuai, System development, formability quality and microstructure evolution of selective laser-melted magnesium, Virtual and Physical Prototyping 11(3) (2016) 173-181.
[45] R. Xu, M.-C. Zhao, Y.-C. Zhao, L. Liu, C. Liu, C. Gao, C. Shuai, A. Atrens, Improved biodegradation resistance by grain refinement of novel antibacterial ZK30-Cu alloys produced via selective laser melting, Materials Letters 237 (2019) 253-257.
[46] F. de Oliveira Campos, A.C. Araujo, A.L. Jardini Munhoz, S.G. Kapoor, The influence of additive manufacturing on the micromilling machinability of Ti6Al4V: A comparison of SLM and commercial workpieces, Journal of Manufacturing Processes 60 (2020) 299-307.
[47] D. Yang, H. Li, S. Liu, C. Song, Y. Yang, S. Shen, J. Lu, Z. Liu, Y. Zhu, In situ capture of spatter signature of SLM process using maximum entropy double threshold image processing method based on genetic algorithm, Optics & Laser Technology 131 (2020) 106371.
[48] T. Larimian, T. Borkar, Additive Manufacturing of In Situ Metal Matrix Composites, in: B. AlMangour ed., Additive Manufacturing of Emerging Materials, Springer International Publishing, Cham, 2019, pp. 1-28.
[49] C. Cai, C. Radoslaw, J. Zhang, Q. Yan, S. Wen, B. Song, Y. Shi, In-situ preparation and formation of TiB/Ti-6Al-4V nanocomposite via laser additive manufacturing: microstructure evolution and tribological behavior, Powder technology 342 (2019) 73-84.
[50] J. Wang, Y. Liu, P. Qin, S. Liang, T. Sercombe, L. Zhang, Selective laser melting of Ti–35Nb composite from elemental powder mixture: Microstructure, mechanical behavior and corrosion behavior, Materials Science and Engineering: A 760 (2019) 214-224.
[51] K. Wei, X. Zeng, Z. Wang, J. Deng, M. Liu, G. Huang, X. Yuan, Selective laser melting of Mg-Zn binary alloys: Effects of Zn content on densification behavior, microstructure, and mechanical property, Materials Science and Engineering: A 756 (2019) 226-236.
[52] T. Long, X. Zhang, Q. Huang, L. Liu, Y. Liu, J. Ren, Y. Yin, D. Wu, H. Wu, Novel Mg-based alloys by selective laser melting for biomedical applications: microstructure evolution, microhardness and in vitro degradation behaviour, Virtual and Physical Prototyping 13(2) (2018) 71-81.
[53] M. Esmaily, Z. Zeng, A.N. Mortazavi, A. Gullino, S. Choudhary, T. Derra, F. Benn, F. D'Elia, M. Müther, S. Thomas, A. Huang, A. Allanore, A. Kopp, N. Birbilis, A detailed microstructural and corrosion analysis of magnesium alloy WE43 manufactured by selective laser melting, Additive Manufacturing 35 (2020) 101321.
[54] N.A. Zumdick, L. Jauer, L.C. Kersting, T.N. Kutz, J.H. Schleifenbaum, D. Zander, Additive manufactured WE43 magnesium: A comparative study of the microstructure and mechanical properties with those of powder extruded and as-cast WE43, Materials Characterization 147 (2019) 384-397.
[55] J. Chen, P. Wu, Q. Wang, Y. Yang, S. Peng, Y. Zhou, C. Shuai, Y. Deng, Influence of alloying treatment and rapid solidification on the degradation behavior and mechanical properties of Mg, Metals 6(11) (2016) 259.
[56] C. Shuai, Y. Yang, S. Peng, C. Gao, P. Feng, J. Chen, Y. Liu, X. Lin, S. Yang, F. Yuan, Nd-induced honeycomb structure of intermetallic phase enhances the corrosion resistance of Mg alloys for bone implants, Journal of Materials Science: Materials in Medicine 28(9) (2017) 130.
[57] C.L. Wu, W. Zai, H.C. Man, Additive manufacturing of ZK60 magnesium alloy by selective laser melting: Parameter optimization, microstructure and biodegradability, Materials Today Communications 26 (2021) 101922.
[58] C. Shuai, L. Liu, M. Zhao, P. Feng, Y. Yang, W. Guo, C. Gao, F. Yuan, Microstructure, biodegradation, antibacterial and mechanical properties of ZK60-Cu alloys prepared by selective laser melting technique, Journal of Materials Science & Technology 34(10) (2018) 1944-1952.
[59] B.R. Sunil, T.S. Kumar, U. Chakkingal, V. Nandakumar, M. Doble, Friction stir processing of magnesium–nanohydroxyapatite composites with controlled in vitro degradation behavior, Materials Science and Engineering: C 39 (2014) 315-324.
[60] R. Del Campo, B. Savoini, A. Muñoz, M. Monge, G. Garcés, Mechanical properties and corrosion behavior of Mg–HAP composites, Journal of the mechanical behavior of biomedical materials 39 (2014) 238-246.
[61] C. Shuai, Y. Zhou, Y. Yang, P. Feng, L. Liu, C. He, M. Zhao, S. Yang, C. Gao, P. Wu, Biodegradation resistance and bioactivity of hydroxyapatite enhanced Mg-Zn composites via selective laser melting, Materials 10(3) (2017) 307.
[62] C. Liu, M. Zhang, C. Chen, Effect of laser processing parameters on porosity, microstructure and mechanical properties of porous Mg-Ca alloys produced by laser additive manufacturing, Materials Science and Engineering: A 703 (2017) 359-371.
[63] X. Yao, J. Tang, Y. Zhou, A. Atrens, M.S. Dargusch, B. Wiese, T. Ebel, M. Yan, Surface modification of biomedical Mg-Ca and Mg-Zn-Ca alloys using selective laser melting: Corrosion behaviour, microhardness and biocompatibility, Journal of Magnesium and Alloys 9(6) (2020) 2155-2168.
[64] S.L. Sing, W.Y. Yeong, F.E. Wiria, Selective laser melting of titanium alloy with 50 wt% tantalum: Microstructure and mechanical properties, Journal of Alloys and Compounds 660 (2016) 461-470.
[65] R. Rahmani, M. Brojan, M. Antonov, K.G. Prashanth, Perspectives of metal-diamond composites additive manufacturing using SLM-SPS and other techniques for increased wear-impact resistance, International Journal of Refractory Metals and Hard Materials 88 (2020) 105192.
[66] N. Putra, M. Mirzaali, I. Apachitei, J. Zhou, A. Zadpoor, Multi-material additive manufacturing technologies for Ti-, Mg-, and Fe-based biomaterials for bone substitution, Acta Biomaterialia 109 (2020) 1-20.
[67] R. Singh, A. Gupta, O. Tripathi, S. Srivastava, B. Singh, A. Awasthi, S.K. Rajput, P. Sonia, P. Singhal, K.K. Saxena, Powder bed fusion process in additive manufacturing: An overview, Materials Today: Proceedings 26 (2020) 3058-3070.
[68] S.M.J. Razavi, B. Van Hooreweder, F. Berto, Effect of build thickness and geometry on quasi-static and fatigue behavior of Ti-6Al-4V produced by Electron Beam Melting, Additive Manufacturing 36 (2020) 101426.
[69] J. Parthasarathy, B. Starly, S. Raman, A. Christensen, Mechanical evaluation of porous titanium (Ti6Al4V) structures with electron beam melting (EBM), Journal of the mechanical behavior of biomedical materials 3(3) (2010) 249-259.
[70] A. Casadebaigt, J. Hugues, D. Monceau, High temperature oxidation and embrittlement at 500–600° C of Ti-6Al-4V alloy fabricated by Laser and Electron Beam Melting, Corrosion Science 175 (2020) 108875.
[71] V. Lunetto, M. Galati, L. Settineri, L. Iuliano, Unit process energy consumption analysis and models for Electron Beam Melting (EBM): Effects of process and part designs, Additive Manufacturing 33 (2020) 101115.
[72] M. Cronskär, M. Bäckström, L.E. Rännar, Production of customized hip stem prostheses–a comparison between conventional machining and electron beam melting (EBM), Rapid Prototyping Journal 19(5) (2013) 365-372.
[73] M. Touri, F. Kabirian, M. Saadati, S. Ramakrishna, M. Mozafari, Additive manufacturing of biomaterials− the evolution of rapid prototyping, Advanced Engineering Materials 21(2) (2019) 1800511.
[74] B.R. Luce, M. Drummond, B. Jönsson, P.J. Neumann, J.S. Schwartz, U. Siebert, S.D. Sullivan, EBM, HTA, and CER: clearing the confusion, The Milbank

Quarterly 88(2) (2010) 256-276.
[75] L.E. Rännar, A. Glad, C.G. Gustafson, Efficient cooling with tool inserts manufactured by electron beam melting, Rapid Prototyping Journal 13(3) (2007) 128-135.
[76] G. Manivasagam, D. Dhinasekaran, A. Rajamanickam, Biomedical implants: corrosion and its prevention-a review, Recent patents on corrosion science 2 (2010) 40-54.
[77] M. Radmansouri, E. Bahmani, E. Sarikhani, K. Rahmani, F. Sharifianjazi, M. Irani, Doxorubicin hydrochloride - Loaded electrospun chitosan/cobalt ferrite/titanium oxide nanofibers for hyperthermic tumor cell treatment and controlled drug release, International Journal of Biological Macromolecules 116 (2018) 378-384.
[78] B. Gao, S. Hao, J. Zou, W. Wu, G. Tu, C. Dong, Effect of high current pulsed electron beam treatment on surface microstructure and wear and corrosion resistance of an AZ91HP magnesium alloy, Surface and Coatings Technology 201(14) (2007) 6297-6303.
[79] D. Schmid, J. Renza, M.F. Zaeh, J. Glasschroeder, Process influences on laser-beam melting of the magnesium alloy AZ91, Physics Procedia 83 (2016) 927-936.
[80] X. Tong, D. Zhang, X. Zhang, Y. Su, Z. Shi, K. Wang, J. Lin, Y. Li, J. Lin, C. Wen, Microstructure, mechanical properties, biocompatibility, and in vitro corrosion and degradation behavior of a new Zn–5Ge alloy for biodegradable implant materials, Acta biomaterialia 82 (2018) 197-204.
[81] M.-S. Song, R.-C. Zeng, Y.-F. Ding, R.W. Li, M. Easton, I. Cole, N. Birbilis, X.-B. Chen, Recent advances in biodegradation controls over Mg alloys for bone fracture management: a review, Journal of materials science & technology 35(4) (2019) 535-544.
[82] E. Sharifi Sedeh, S. Mirdamadi, F. Sharifianjazi, M. Tahriri, Synthesis and Evaluation of Mechanical and Biological Properties of Scaffold Prepared From Ti and Mg With Different Volume Percent, Synthesis and Reactivity in Inorganic, Metal-Organic, and Nano-Metal Chemistry 45(7) (2015) 1087-1091.
[83] M. Vlasea, Y. Shanjani, A. Basalah, E. Toyserkani, Additive manufacturing of scaffolds for tissue engineering of bone and cartilage, International Journal of Advanced Manufacturing Technology 13(1) (2011) 124-141.
[84] R. Narayan, Fundamentals of medical implant materials, ASM handbook Volume 23: Materials for Medical Devices, ASM International, United States of America (USA), 2012.
[85] L. Shi, L. Wang, Y. Duan, W. Lei, Z. Wang, J. Li, X. Fan, X. Li, S. Li, Z. Guo, The improved biological performance of a novel low elastic modulus implant, PLoS one 8(2) (2013) e55015.
[86] L.J. Gibson, Biomechanics of cellular solids, Journal of biomechanics 38(3) (2005) 377-399.
[87] E. O. Hall, Yield point phenomena in metals and alloys, First ed. 1970, Springer, New York, 2012.
[88] S.L. Sing, L.P. Lam, D.Q. Zhang, Z.H. Liu, C.K. Chua, Interfacial characterization of SLM parts in multi-material processing: Intermetallic phase formation between AlSi10Mg and C18400 copper alloy, Materials Characterization 107 (2015) 220-227.
[89] Y. Qin, P. Wen, H. Guo, D. Xia, Y. Zheng, L. Jauer, R. Poprawe, M. Voshage, J.H. Schleifenbaum, Additive manufacturing of biodegradable metals: current research status and future perspectives, Acta biomaterialia 98 (2019) 3-22.
[90] Y. Qin, P. Wen, M. Voshage, Y. Chen, P.G. Schückler, L. Jauer, D. Xia, H. Guo, Y. Zheng, J.H. Schleifenbaum, Additive manufacturing of biodegradable Zn-xWE43 porous scaffolds: Formation quality, microstructure and mechanical properties, Materials & Design 181 (2019) 107937.
[91] Y. Li, J. Zhou, P. Pavanram, M. Leeflang, L. Fockaert, B. Pouran, N. Tümer, K.-U. Schröder, J. Mol, H. Weinans, Additively manufactured biodegradable porous magnesium, Acta biomaterialia 67 (2018) 378-392.
[92] F. Witte, The history of biodegradable magnesium implants: a review, Acta biomaterialia 6(5) (2010) 1680-1692.
[93] D. Mareci, G. Bolat, J. Izquierdo, C. Crimu, C. Munteanu, I. Antoniac, R. Souto, Electrochemical characteristics of bioresorbable binary MgCa alloys in Ringer's solution: Revealing the impact of local pH distributions during in-vitro dissolution, Materials Science and Engineering: C 60 (2016) 402-410.
[94] P. Abasian, M. Radmansouri, M. Habibi Jouybari, M.V. Ghasemi, A. Mohammadi, M. Irani, F.S. Jazi, Incorporation of magnetic NaX zeolite/DOX into the PLA/chitosan nanofibers for sustained release of doxorubicin against carcinoma cells death in vitro, International Journal of Biological Macromolecules 121 (2019) 398-406.
[95] R. Radha, D. Sreekanth, Insight of magnesium alloys and composites for orthopedic implant applications–a review, Journal of magnesium and alloys 5(3) (2017) 286-312.
[96] J. Kubasek, D. Dvorsky, M. Cavojsky, M. Roudnicka, D. Vojtech, WE43 magnesium alloy-material for challenging applications, Kovove Materialy 57(3) (2019) 159-165.
[97] J. Trinidad, I. Marco, G. Arruebarrena, J. Wendt, D. Letzig, E. Sáenz de Argandoña, R. Goodall, Processing of magnesium porous structures by infiltration casting for biomedical applications, Advanced Engineering Materials 16(2) (2014) 241-247.
[98] S. Gollapudi, Grain size distribution effects on the corrosion behaviour of materials, Corrosion Science 62 (2012) 90-94.
[99] X. Zhao, L.-l. Shi, J. Xu, A comparison of corrosion behavior in saline environment: rare earth metals (Y, Nd, Gd, Dy) for alloying of biodegradable magnesium alloys, Journal of Materials Science & Technology 29(9) (2013) 781-787.
[100] Z. Zhen, T.-f. Xi, Y.-f. Zheng, A review on in vitro corrosion performance test of biodegradable metallic materials, Transactions of Nonferrous Metals Society of China 23(8) (2013) 2283-2293.
[101] X. Niu, H. Shen, J. Fu, J. Yan, Y. Wang, Corrosion behaviour of laser powder bed fused bulk pure magnesium in hank's solution, Corrosion Science 157 (2019) 284-294.
[102] G. Argade, S. Panigrahi, R. Mishra, Effects of grain size on the corrosion resistance of wrought magnesium alloys containing neodymium, Corrosion Science 58 (2012) 145-151.
[103] J. Zhang, B. Song, Q. Wei, D. Bourell, Y. Shi, A review of selective laser melting of aluminum alloys: Processing, microstructure, property and developing trends, Journal of Materials Science & Technology 35(2) (2019) 270-284.
[104] B. Xie, M.-C. Zhao, Y.-C. Zhao, Y. Tian, D. Yin, C. Gao, C. Shuai, A. Atrens, Effect of Alloying Mn by Selective Laser Melting on the Microstructure and Biodegradation Properties of Pure Mg, Metals 10(11) (2020) 1527.
[105] C. Shuai, Y. Yang, P. Wu, X. Lin, Y. Liu, Y. Zhou, P. Feng, X. Liu, S. Peng, Laser rapid solidification improves corrosion behavior of Mg-Zn-Zr alloy, Journal of Alloys and Compounds 691 (2017) 961-969.
[106] R. K.R, S. Bontha, R. M.R, M. Das, V.K. Balla, Laser surface melting of Mg-Zn-Dy alloy for better wettability and corrosion resistance for biodegradable implant applications, Applied Surface Science 480 (2019) 70-82.
[107] M. Gieseke, C. Noelke, S. Kaierle, V. Wesling, H. Haferkamp, Selective Laser Melting of Magnesium and Magnesium Alloys, in: N. Hort, S.N. Mathaudhu, N.R. Neelameggham, M. Alderman (Eds.), Magnesium Technology 2013, Springer International Publishing, Cham, 2016, pp. 65-68.
[108] C. Shuai, Y. Cheng, Y. Yang, S. Peng, W. Yang, F. Qi, Laser additive manufacturing of Zn-2Al part for bone repair: Formability, microstructure and properties, Journal of Alloys and Compounds 798 (2019) 606-615.
[109] Y. Yang, X. Guo, C. He, C. Gao, C. Shuai, Regulating degradation behavior by incorporating mesoporous silica for Mg bone implants, ACS Biomaterials Science & Engineering 4(3) (2018) 1046-1054.
[110] M.M. Saleh, A. Touny, M.A. Al-Omair, M. Saleh, Biodegradable/biocompatible coated metal implants for orthopedic applications, Bio-medical materials and engineering 27(1) (2016) 87-99.
[111] Y. Ding, C. Wen, P. Hodgson, Y. Li, Effects of alloying elements on the corrosion behavior and biocompatibility of biodegradable magnesium alloys: a review, Journal of materials chemistry B 2(14) (2014) 1912-1933.
[112] K. Munir, J. Lin, C. Wen, P.F. Wright, Y. Li, Mechanical, corrosion, and biocompatibility properties of Mg-Zr-Sr-Sc alloys for biodegradable implant applications, Acta biomaterialia 102 (2020) 493-507.
[113] M. Rahman, N.K. Dutta, N. Roy Choudhury, Magnesium Alloys With Tunable Interfaces as Bone Implant Materials, Frontiers in Bioengineering and Biotechnology 8 (2020) 564.
[114] A.H.M. Sanchez, B.J. Luthringer, F. Feyerabend, R. Willumeit, Mg and Mg alloys: how comparable are in vitro and in vivo corrosion rates? A review, Acta biomaterialia 13 (2015) 16-31.
[115] C. Xiao, L. Wang, Y. Ren, S. Sun, E. Zhang, C. Yan, Q. Liu, X. Sun, F. Shou, J. Duan, Indirectly extruded biodegradable Zn-0.05 wt% Mg alloy with improved strength and ductility: In vitro and in vivo studies, Journal of materials science & technology 34(9) (2018) 1618-1627.
[116] L. Murr, Metallurgy principles applied to powder bed fusion 3D printing/additive manufacturing of personalized and optimized metal and alloy biomedical implants: An overview, Journal of Materials Research and Technology 9(1) (2020) 1087-1103.
[117] M. Farag, H.-s. Yun, Effect of gelatin addition on fabrication of magnesium phosphate-based scaffolds prepared by additive manufacturing system, Materials Letters 132 (2014) 111-115.
[118] M. Castilho, M. Dias, U. Gbureck, J. Groll, P. Fernandes, I. Pires, B. Gouveia, J. Rodrigues, E. Vorndran, Fabrication of computationally designed scaffolds by low temperature 3D printing, Biofabrication 5(3) (2013) 035012.
[119] Y. Yin, Q. Huang, L. Liang, X. Hu, T. Liu, Y. Weng, T. Long, Y. Liu, Q. Li,

S. Zhou, In vitro degradation behavior and cytocompatibility of ZK30/bioactive glass composites fabricated by selective laser melting for biomedical applications, Journal of Alloys and Compounds 785 (2019) 38-45.
[120] F. Sharifianjazi, N. Parvin, M. Tahriri, Synthesis and characteristics of sol-gel bioactive SiO_2-P_2O_5-CaO-Ag_2O glasses, Journal of Non-Crystalline Solids 476 (2017) 108-113.
[121] F. Bär, L. Berger, L. Jauer, G. Kurtuldu, R. Schäublin, J.H. Schleifenbaum, J.F. Löffler, Laser additive manufacturing of biodegradable magnesium alloy WE43: A detailed microstructure analysis, Acta Biomaterialia 98 (2019) 36-49.
[122] A.C. Hänzi, P. Gunde, M. Schinhammer, P.J. Uggowitzer, On the biodegradation performance of an Mg–Y–RE alloy with various surface conditions in simulated body fluid, Acta biomaterialia 5(1) (2009) 162-171.
[123] C. Gao, S. Li, L. Liu, S. Bin, Y. Yang, S. Peng, C. Shuai, Dual alloying improves the corrosion resistance of biodegradable Mg alloys prepared by selective laser melting, Journal of Magnesium and Alloys 9(1) (2020) 305-316.
[124] M. Li, F. Benn, T. Derra, N. Kröger, M. Zinser, R. Smeets, J.M. Molina-Aldareguia, A. Kopp, J. Llorca, Microstructure, mechanical properties, corrosion resistance and cytocompatibility of WE43 Mg alloy scaffolds fabricated by laser powder bed fusion for biomedical applications, Materials Science and Engineering: C 119 (2021) 111623.
[125] C. Shuai, S. Li, C. Gao, Y. Yang, Z. Zhao, W. Liu, Y. Hu, Supersaturated Solid Solution of Mg in Fe Produced by Mechanical Alloying Followed by Selective Laser Melting (SLM) to Accelerate Degradation for Biomedical Applications, Lasers in Engineering (Old City Publishing) 47(4-6) (2020) 375-391.
[126] G.K. Meenashisundaram, N. Wang, S. Maskomani, S. Lu, S.K. Anantharajan, S.T. Dheen, S.M.L. Nai, J.Y.H. Fuh, J. Wei, Fabrication of Ti + Mg composites by three-dimensional printing of porous Ti and subsequent pressureless infiltration of biodegradable Mg, Materials Science and Engineering: C 108 (2020) 110478.
[127] B. Ghotbi, S. Navkhasi, S. Ghobadi, Z. Shahsavari, N. Kahrizi, A Review of the Novel Corona Virus Disease (2019-nCoV), Health Research Journal 5(3) (2020) 180-187.
[128] M. Salehi, S. Maleksaeedi, M.A.B. Sapari, M.L.S. Nai, G.K. Meenashisundaram, M. Gupta, Additive manufacturing of magnesium–zinc–zirconium (ZK) alloys via capillary-mediated binderless three-dimensional printing, Materials & Design 169 (2019) 107683.
[129] S. Liu, W. Yang, X. Shi, B. Li, S. Duan, H. Guo, J. Guo, Influence of laser process parameters on the densification, microstructure, and mechanical properties of a selective laser melted AZ61 magnesium alloy, Journal of Alloys and Compounds 808 (2019) 151160.
[130] N. Wegner, D. Kotzem, Y. Wessarges, N. Emminghaus, C. Hoff, J. Tenkamp, J. Hermsdorf, L. Overmeyer, F. Walther, Corrosion and Corrosion Fatigue Properties of Additively Manufactured Magnesium Alloy WE43 in Comparison to Titanium Alloy Ti-6Al-4V in Physiological Environment, Materials 12(18) (2019) 2892.